

Optimized $K\alpha$ x-ray flashes from femtosecond-laser-irradiated foils

W. Lu, M. Nicoul, U. Shymanovich, A. Tarasevitch, P. Zhou, K. Sokolowski-Tinten, and D. von der Linde
Institut für Experimentelle Physik, Universität Duisburg-Essen, D-47048 Duisburg, Germany

M. Mašek

Institute of Physics, Academy of Sciences of the Czech Republic, Prague, Czech Republic

P. Gibbon

Institute for Advanced Simulation, Jülich Supercomputing Centre, Forschungszentrum Jülich GmbH, D-52425 Jülich, Germany

U. Teubner*

*Fachbereich Technik, Abt. Naturwiss. Technik, Bereich Photonik, Fachhochschule Oldenburg/Ostfriesland/Wilhelmshaven,
 University of Applied Sciences, Constantiaplatz 4, 26723 Emden, Germany
 and Institut für Physik, Carl von Ossietzky Universität Oldenburg, 26111 Oldenburg, Germany*

(Received 19 March 2009; published 27 August 2009)

We investigate the generation of ultrashort $K\alpha$ pulses from plasmas produced by intense femtosecond p -polarized laser pulses on Copper and Titanium targets. Particular attention is given to the interplay between the angle of incidence of the laser beam on the target and a controlled prepulse. It is observed experimentally that the $K\alpha$ yield can be optimized for correspondingly different prepulse and plasma scale-length conditions. For steep electron-density gradients, maximum yields can be achieved at larger angles. For somewhat expanded plasmas expected in the case of laser pulses with a relatively poor contrast, the $K\alpha$ yield can be enhanced by using a near-normal-incidence geometry. For a certain scale-length range (between 0.1 and 1 times a laser wavelength) the optimized yield is scale-length independent. Physically this situation arises because of the strong dependence of collisionless absorption mechanisms—in particular resonance absorption—on the angle of incidence and the plasma scale length, giving scope to optimize absorption and hence the $K\alpha$ yield. This qualitative description is supported by calculations based on the classical resonance absorption mechanism and by particle-in-cell simulations. Finally, the latter simulations also show that even for initially steep gradients, a rapid profile expansion occurs at oblique angles in which ions are pulled back toward the laser by hot electrons circulating at the front of the target. The corresponding enhancement in $K\alpha$ yield under these conditions seen in the present experiment represents strong evidence for this suprathermal shelf formation effect.

DOI: [10.1103/PhysRevE.80.026404](https://doi.org/10.1103/PhysRevE.80.026404)

PACS number(s): 52.38.Ph, 52.38.Dx, 52.50.Jm, 52.65.-y

I. INTRODUCTION

The control and optimization of the x-ray emission from plasmas produced by high intensity laser-solid interaction is a subject of strong current interest [1–8]. A particularly strong motivation is to use an optimized femtosecond-laser plasma x-ray source for applications such as time-resolved x-ray diffraction (TRXD) [9].

The interaction of a high intensity laser beam with a solid surface rapidly creates a plasma, subsequently leading to emission of a short burst of x-rays. According to current understanding, the electrons in the surface plasma are accelerated by the strong electric field of the laser and then penetrate into the solid behind. There, they knock out electrons from inner electronic shells, which subsequently undergo inner-shell recombination, leading to characteristic line emission. In this process, the velocity distribution of the high-energy electrons strongly influences the characteristics of the emitted radiation, in particular the $K\alpha$ and $K\beta$ x-ray yield. This hot-electron distribution is in turn determined by the

parameters of the driving laser, i.e., intensity, angle of incidence, laser polarization, as well as the properties of the plasma with which the laser pulse interacts.

The dependence of fast electron energy on the laser field means that the laser intensity is one of the key factors for optimization of $K\alpha$ emission. The average energy of the accelerated electrons generally follows a power scaling law as a function of the product of the laser intensity and the wavelength squared ($I_0\lambda^2$) [1–4]. For optimal $K\alpha$ emission, the average electron energy, often described by an effective hot-electron temperature T_h , should be few times the K -shell ionization energy, depending on the atomic number and geometry of the target [5–7]. These considerations allow the laser intensity for optimum $K\alpha$ production to be estimated. For example, to maximize the yield of Cu $K\alpha$ radiation, the average electron energy should be between 25 and 50 keV [1,5,10–12]. From the scaling law it follows that this average electron energy corresponds to a laser intensity of a few times 10^{17} W/cm² at a laser wavelength of 800 nm; for Ti, the optimal laser intensity is about 10^{16} W/cm² [5].

Another key factor for optimization of the $K\alpha$ emission is the conversion efficiency, which is a function of the energy converted from the laser pulse to electrons in the required energy range and subsequently from hot electrons to the $K\alpha$

*Corresponding author; teubner@nwt.fho-emden.de

photons. There is no simple scaling law for this process [1]. The dominant absorption mechanism at laser intensities from 10^{16} to 10^{17} W/cm² is expected to be resonance absorption (RA) [5,13–19]. The crucial parameter for the efficiency of the energy transfer for this mechanism is the plasma scale length at the time when the maximum intensity is reached. Therefore, the conversion efficiency is very sensitive to the temporal structure of the rising edge of the laser pulse. Since the plasma expands with a typical velocity of a few times 10^7 cm/s, the time interval between the plasma-formation threshold and the maximum intensity largely determines the scale length seen by the pulse during the interaction. In most laser systems, the prepulse and/or amplified spontaneous emissions (ASE) usually cause plasma formation. For this reason, control over the time structure of the pulse provided by the laser system becomes important to control the $K\alpha$ emission. An important measurement of the laser-pulse time structure is the contrast ratio, defined as the ratio of the pulse in maximum and prepulse before the main pulse. In some previous work [13,14,20,21], the time structure of the laser pulses provided by the laser systems were already producing scale lengths conducive to high absorption, making additional improvements difficult. However, relying on the system prepulse alone for “optimization” is hardly satisfactory: the scale length will rarely be matched to other parameters. It has already been demonstrated that a weak artificial prepulse can increase the conversion efficiency of the x-ray yield from laser produced plasma [7,22–27]. Generally, however, the initial scale length is too short for the main pulse parameters, which is why systematic investigations of plasma scale length requirements for different experimental conditions are necessary. A controlled prepulse can generate a preformed plasma with specific density scale lengths matched to the absorption mechanism likely to dominate when the main pulse arrives. This offers the possibility of actively manipulating the coupling efficiency, hot-electron distribution, and thus the $K\alpha$ emission.

In this study we investigated the $K\alpha$ emission of Ti and Cu targets for different excitation and plasma conditions. We present measurements of the $K\alpha$ yield as a function of target thickness and angle of incidence, and investigate the influence of a preplasma in detail by using a controlled prepulse with variable delay. It is found that with a suitable preplasma, the $K\alpha$ production on both targets can be improved. A one-dimensional particle-in-cell (PIC) code is applied to model the experimental results, and gives a broad nearly quantitative agreement between the simulations and measurements. Additionally, both experimental results and simulations show that the resonance absorption mechanism is the dominant absorption mechanism in our experiment.

II. EXPERIMENTAL SETUP

The experiments were carried out with a chirped pulse amplification (CPA) Ti:sapphire laser system delivering 150 fs pulses at a wavelength of 800 nm with an energy of 120 mJ and a repetition rate of 10 Hz. The time structure of the laser was measured using a fast photodiode (ns time range) and a third-order autocorrelator (fs to ps time range). The

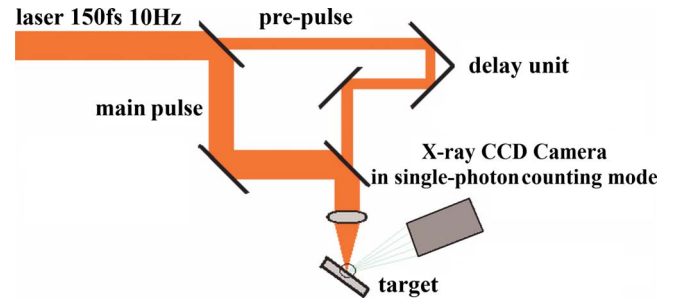


FIG. 1. (Color online) Schematic of the experimental setup.

amplified laser pulse exhibits a prepulse approximately 1 ps ahead of the pulse maximum with a relative intensity of about 10^{-7} (i.e., contrast ratio of 10^7); the contrast ratio of ASE was 10^8 . A schematic of the experimental setup is shown in Fig. 1. The 25-mm-diameter (FWHM) main laser beam was reflected from a mirror with a 5-mm-diameter hole drilled in its center that allowed transmission of a small part of the beam. The transmitted part was time delayed with a variable delay line, and recombined with the main laser beam, using a second apertured mirror. The combined p -polarized laser beam was focused with a 30-cm focal length lens onto the target surface. This lens could be accurately translated along the direction of the laser beam to change the focusing conditions on the target. By using a microscope objective combined with a charge-coupled device (CCD) camera, we measured the focal spot size of the prepulse to be about 12 times larger than that of the main pulse and both pulses overlapped well at all delay times. The angle of incidence was varied by rotating the target. For each specific angle, the laser intensity was kept constant by adjusting the laser energy. The targets were mounted on a motorized XYZ translation unit and moved between subsequent laser pulses to provide a fresh surface. In these experiments, four kinds of targets have been used: 300-nm Cu and Ti films coated on a glass substrate and 20 μ m Cu and Ti foils glued onto a glass substrate.

The x-ray radiation was detected with a Princeton Instrument PI-MTE: 1300B camera from Roper Scientific. Its back-illuminated CCD is suitable for the energy range of the x-ray photons of the present work. The chip area is 1340 pixels*1300 pixels (20 μ m*20 μ m each). The camera was located \sim 20 cm away from the x-ray source. To allow the camera to work in the single-photon counting mode and to avoid pile-up problems due to the summation of the energy of more than one photon within one pixel [28], the average flux per pulse was reduced to 1 photon per 40 pixels by using an Al filter of moderate thickness (150 μ m and 210 μ m for Ti and Cu, respectively) in front of the camera. The filter also protected the CCD from low-energy Bremsstrahlung and from visible light. Charge spreading on CCD detector has been taken into account.

A typical single-pulse spectrum (after subtraction of a Bremsstrahlung background) using Cu as target, with well resolved Cu $K\alpha$ and $K\beta$ lines at 8.05 and 8.91 keV, respectively, is shown in Fig. 2. The single-pulse spectra of Ti, which are not shown here, are similar. The absolute $K\alpha$ emission yield was derived by integrating the number of $K\alpha$

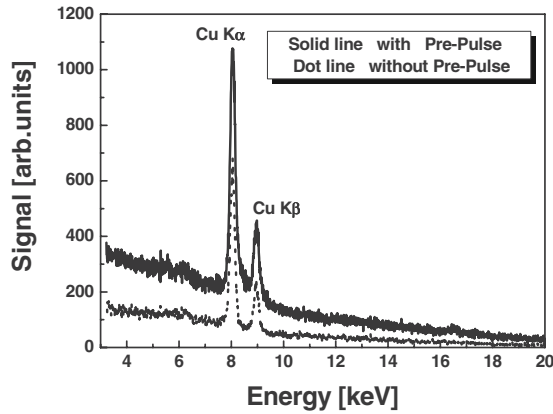


FIG. 2. Spectrum of the laser produced $K\alpha$ emission of Cu.

photons registered by the CCD and calculating the total yield per laser pulse, assuming isotropic emission into 4π steradian, considering the filter transmission and quantum efficiency of the CCD (18% for Cu and 55% for Ti) [29].

III. EXPERIMENTAL RESULTS

Figure 3 shows the experimental results of $K\alpha$ production as a function of the focal position of the focusing lens on Cu and Ti targets, without an additional prepulse. It can be clearly seen that the sharpest focusing provides the largest $K\alpha$ emission for the Cu target, but that a defocused position achieves this for the Ti target. This effect has been discussed before in the literature [13,20,30]. By varying the relative position of the laser focus with respect to the target surface the laser intensity on the target changes, which results in the change in T_h and subsequently affects the x-ray $K\alpha$ yield. Figure 3 indicates that for Ti, an optimum intensity for $K\alpha$ production exists, as predicted by theory [5], which is lower than the maximum laser intensity reached in the focus. For Cu the double-peak structure is not observed because the intensity used is still below the optimal value for this atomic number. For laser energies above 30 mJ and intensities in the

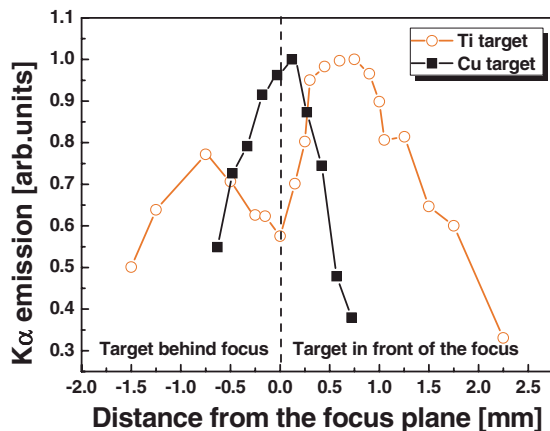


FIG. 3. (Color online) $K\alpha$ emission as a function of the relative position of laser focus respect to the target surface on massive Cu and Ti targets. The lines between the data points are only to guide the eye.

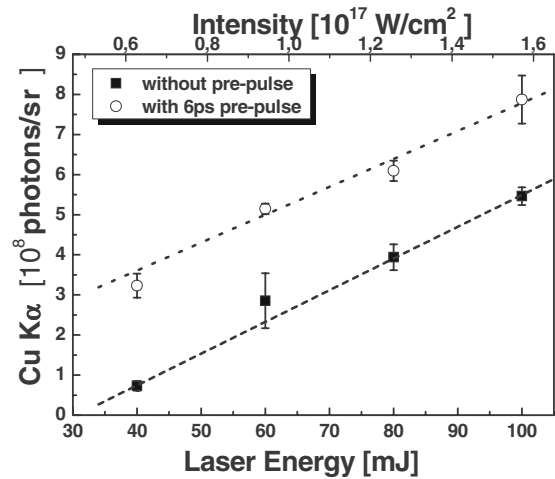


FIG. 4. Measured dependence of x-ray yield on laser energy for a 20 μm Cu foil. The angle of incidence is 45° .

region from 10^{16} W/cm² to 10^{17} W/cm², the $K\alpha$ -yield scales linearly with laser energy/intensity—Fig. 4. There was no evidence of saturation, in agreement with theoretical calculations which predict an optimum intensity for Cu $K\alpha$ production of about 10^{18} W/cm² [7].

In the experiments described in the following, the Cu targets were placed exactly in the focus of the lens, while the Ti targets were placed about 900 μm in front of the focus. These configurations lead to intensities on the Cu and Ti targets of 1.6×10^{17} W/cm² [focus diameter 20 μm full width at half maximum (FWHM)] and 9.2×10^{16} W/cm² (26 μm FWHM) for the main pulse and 2.0×10^{14} W/cm² (70 μm FWHM) and 1.1×10^{14} W/cm² (91 μm FWHM) for the prepulse, respectively.

The normalized Cu and Ti $K\alpha$ emission as a function of the main pulse delay at a fixed angle of incidence of 45° for different target thicknesses are presented in Figs. 5(a) and 5(b), respectively. The data in the figure have been normalized to the emission per pulse measured at negative time delay, which are 5.2×10^8 photons/sr for 20 μm Cu, 8.2×10^7 photons/sr for 300-nm Cu, 1.4×10^9 photons/sr for 20 μm Ti, and 1.2×10^8 photons/sr for 300-nm Ti. The $K\alpha$ yields of the 20 μm targets are six and 11 times larger than for the 300-nm Cu and Ti targets, respectively. This is because at these intensities the mean-free path of the hot electrons is much larger (several microns) than the thin-film sample thickness [5,20,31]. Therefore, in the thin films only a small fraction of all the hot electrons will create a hole in the K shell and thus the $K\alpha$ emission is less than for a bulk target.

In the presence of an extended preplasma created by the prepulse, the $K\alpha$ yields start to improve. After a certain time delay, the $K\alpha$ yields reach their maximum, and start to drop with further increasing delay times. These results show that the preplasma that is generated by the controlled prepulse optimizes laser absorption and permits effective $K\alpha$ production: at angle of incidence of 45° an optimum time delay for $K\alpha$ production exists on all types of targets. Under these optimal conditions, the $K\alpha$ production on all targets is improved by almost a factor of 2; whereby the coating targets

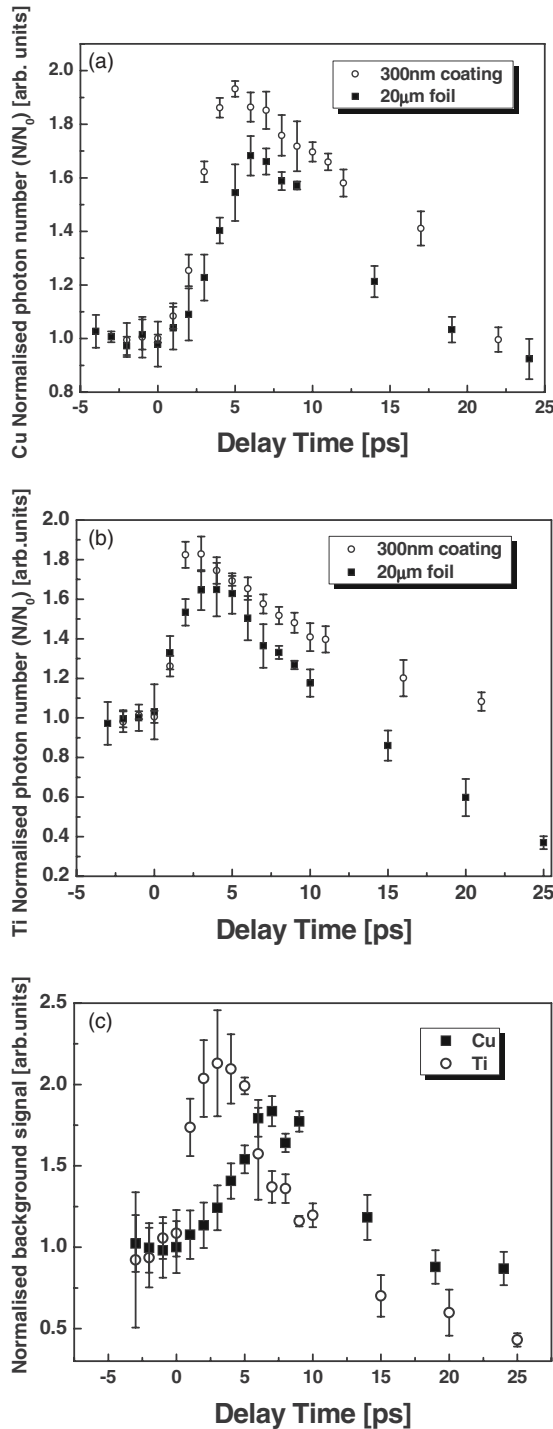


FIG. 5. Normalized $K\alpha$ emissions *per pulse* as a function of main pulse delay at fixed angle of incidence of 45° on different target thickness. (a) Cu-Target, $N_0=5.2 \times 10^8$ photons/sr and 8.2×10^7 photons/sr for $d=20 \mu\text{m}$ and 300 nm, respectively. (b) Ti-Target, $N_0=1.4 \times 10^9$ photons/sr and 1.2×10^8 photons/sr for $d=20 \mu\text{m}$ and 300 nm, respectively. (c) Hard x-ray background signal as a function of main pulse delay on $20 \mu\text{m}$ targets.

see slightly better improvements than the thick foil targets. On the other hand, it has to be noted that the hard x-ray background signal also increased with increasing $K\alpha$ yield. Hard x-ray background signals were calculated by integrat-

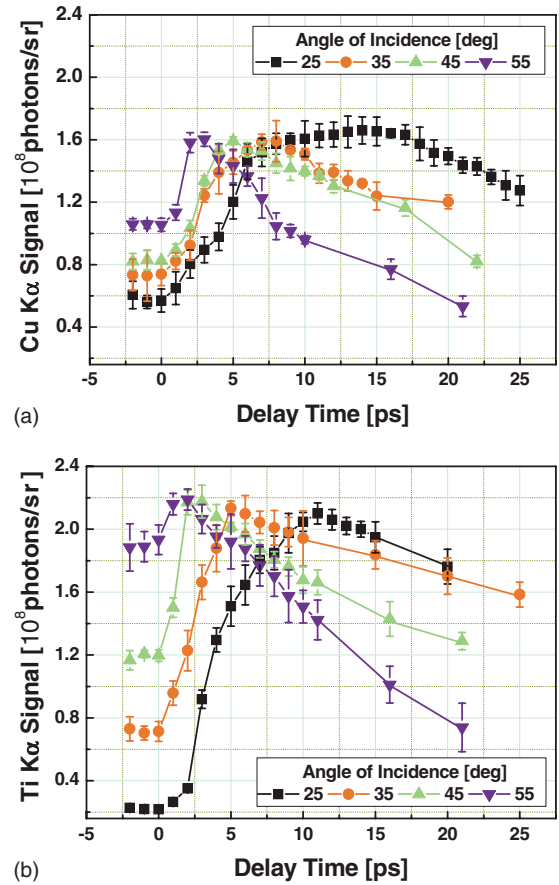


FIG. 6. (Color online) $K\alpha$ emission per pulse as a function of main pulse delay at different angle of incidence, (a) Cu and (b) Ti. The measured $K\alpha$ yield at negative or zero delay is the same as obtained without prepulse.

ing the tail of the single-shot spectra from the CCD in the energy range 6–30 keV for Ti and 10–30 keV for Cu; their dependency on the prepulse delay is shown in Fig. 5(c).

A more systematic study of the influence of a preplasma on the $K\alpha$ production was made by using a controlled prepulse with variable delay. Figures 6(a) and 6(b) show the Cu and Ti $K\alpha$ emission as a function of the main pulse delay at different angles of incidence, respectively. In these measurements, we used 300-nm coating films as targets because of their high-quality surface for the formation of plasma, although as we already noted above, the absolute $K\alpha$ yields are less than for the $20 \mu\text{m}$ foil target. Introducing prepulse results in an increase in the $K\alpha$ yield, which is particularly important for small angles of incidence. The $K\alpha$ yield of both target elements exhibit similar qualitative dependencies on delay time and angle of incidence, though the Ti target shows noticeably larger relative variations.

IV. DISCUSSION

Due to the high-contrast ratio laser pulse in the present experiment, the scale length in the *absence* of a controlled prepulse will be negligible. For any collisionless absorption mechanism, at short scale lengths the angle-of-incidence α

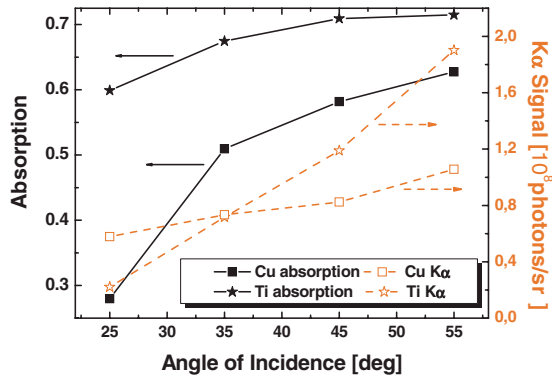


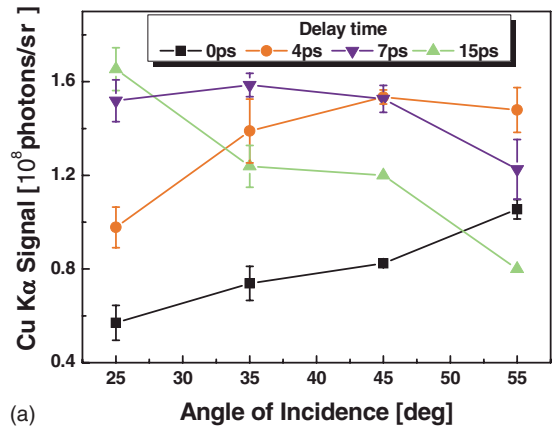
FIG. 7. (Color online) Absorption measurement with main pulse only, measured at the constant laser intensity. Scale on left-hand side: absorption, scale on right-hand side: Cu and Ti $K\alpha$ yield at $\Delta t=0$ (data taken from Fig. 6).

where the absorption is maximum (i.e., α_{\max}) occurs at a large value [32–34], typically 70° or 80° . In such a case the absorption should increase monotonically with the angle of incidence and this is expected to result in an increase in $K\alpha$ yield. In Fig. 7, the absorption measurements with the main pulse and the Cu and Ti $K\alpha$ yield at $\Delta t=0$ from Fig. 6 are presented together. The measurement was carried out at constant laser intensity ($\sim 1.6 \times 10^{17}$ W/cm 2 for Cu and $\sim 9.2 \times 10^{16}$ W/cm 2 for Ti). As seen from Fig. 7, the absorption of laser energy does indeed increase with the angle of incidence for both target elements. As expected, the $K\alpha$ yields of both elements also increase monotonically with α , indicating that $K\alpha$ can be generated quite efficiently at large angles of incidence.

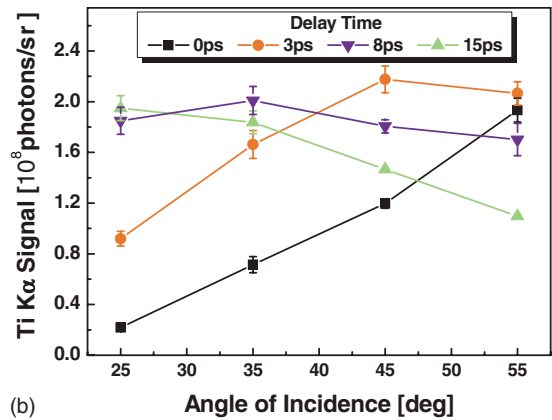
From the data of Fig. 6 we can deduce the dependence of $K\alpha$ yield as a function of the angle of incidence. This is plotted in Fig. 8 for different fixed prepulse delay times Δt . For the present experimental conditions, Δt essentially represents the value of the plasma scale-length L and thus the data plotted in Fig. 8 show the $K\alpha$ yields as a function of the angle of incidence for different plasma scale lengths. For $\Delta t=0$ ps (very short scale length), the $K\alpha$ yield increases monotonically with α . The maximum of $K\alpha$ yield is somewhere beyond 55° . When the delay Δt (scale length) is increased, the maximum $K\alpha$ yield shifts to a smaller angle of incidence, e.g., in (a) for $\Delta t=4$ ps the maximum appears at 45° ; for $\Delta t=7$ ps at 35° . Finally, for $\Delta t=15$ ps, the $K\alpha$ yield decreases monotonically with α . The maximum of $K\alpha$ yield shifts to less than 25° . As discussed above, the maximum $K\alpha$ yields are correlated with the absorption maxima, which in turn shift to small angles of incidence due to the prepulse effect.

In Fig. 9, the Cu and Ti $K\alpha$ yields at the optimum delay (for the corresponding α) and at negative delay ($\Delta t < 0$ ps) have been extracted from Fig. 6. At negative delay (where the prepulse arrives after the main pulse and thus does not play a role), the yield increases with the angle of incidence. On the contrary, at the optimum delay (optimum plasma scale length) the $K\alpha$ yield is essentially independent of the angle of incidence.

In the case of Cu and $\Delta t=0$ ps (or negative), the peak may occur at large angle of incidence. Thus starting at this



(a)



(b)

FIG. 8. (Color online) $K\alpha$ emission per pulse as a function of the angle of incidence at fixed prepulse delay. a) Cu at $\Delta t=0, 4, 7$, and 15 ps. b) Ti at similar delay times.

angle and then decreasing α , it leads to a decrease in the $K\alpha$ yield as indicated by the dashed-dotted line, i.e., $K\alpha$ generation becomes more and more inefficient. However, this can be fully compensated (i.e., the yield can be shifted back onto the solid line) by an appropriate prepulse. In particular, at small angle of incidence this requires a large delay (which leads to a relatively long scale length for the interaction of

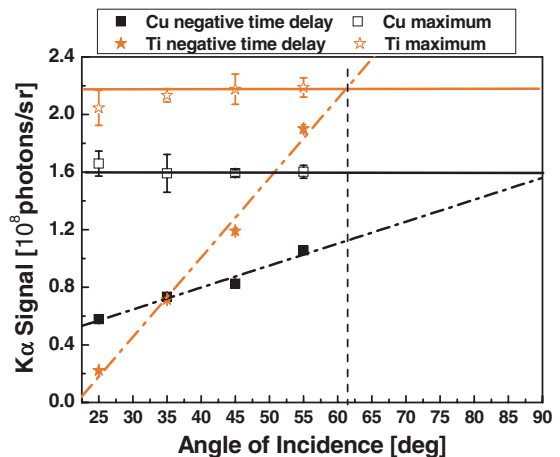


FIG. 9. (Color online) Cu and Ti $K\alpha$ yield per pulse at the maximum peak and at negative time delay (or without prepulse). The lines are to guide the eye only.

the main pulse, see also discussion below), or a somewhat smaller Δt at intermediate α .

For Ti the situation is partly different: again, the $K\alpha$ yield is essentially independent of the angle of incidence, but the intersection of the solid and the dashed-dotted line does not occur at large α (i.e., in the vicinity of $\sim 80^\circ$), but at approximately 60° . This result might arise from the presence of a short scale length preplasma caused by the main pulse itself (even for a high-contrast laser pulse and in the absence of any further prepulse). As discussed for the absorption in Fig. 7, it indicates that at this large angle the self-generated plasma scale length from the main pulse fulfills the optimal condition for $K\alpha$ generation for the present experiment. Hence, the optimized $K\alpha$ yield can be obtained without introducing an artificial prepulse—a conclusion which is also supported by PIC simulations (see Sec. V). This would also explain why in many experiments even a bad contrast ratio leads to high $K\alpha$ generation, especially if α has been chosen small enough [13,14,20,21].

Under conditions specific for the present experiment, RA is expected to be the dominant absorption mechanism. A simple theoretical estimate of the optimal plasma scale length for RA [33] can be found from the formula: $(2\pi L/\lambda)^{2/3} \sin^2 \alpha_{\max} = 0.6$, where L/λ is the scale length normalized to the laser wavelength. For angles-of-incidence 55° , 45° , 35° , and 25° , the optimal normalized scale lengths are 0.135, 0.209, 0.392, and 0.980, respectively. In the present work, the plasma scale length was modified by a controlled laser prepulse at various delay times relative to the laser main pulse. It grows according to $L \equiv C_s \Delta t$ [35], where Δt is the delay between the prepulse and the main pulse, and $C_s = (ZkT_e/M)^{1/2}$ is the expansion velocity of the plasma. T_e is the electron temperature (also determined by the prepulse intensity), Z is the average ionization degree, k is the Boltzmann constant, and M is the ion mass. When the prepulse laser intensity is constant, we can assume that L is approximately proportional to Δt . For this reason, although the absolute values of the scale length were not measured in the experiment, we are still able to deduce the relative values from these data and compare them to the theoretical estimates. For this estimate we assume that both, the process, how the laser light is coupled to the plasma (i.e., RA), and how it is converted to x-rays later on [19], are optimized. This includes optimization of the number of electrons relevant for $K\alpha$ production and the conversion to $K\alpha$ photons as discussed in Sec. V. Both effects are optimized at the same time.

In Fig. 10(a), the optimal delay times of the prepulse for maximum $K\alpha$ emission in Fig. 6 are shown. The maxima appeared at about 3, 5, 8, and 15 ps on the Cu target at 55° , 45° , 35° , and 25° , respectively. For Ti, they were at about 2, 3, 5, and 11 ps at 55° , 45° , 35° , and 25° , respectively. Figure 10(b) displays the optimum delay time from Fig. 10(a) normalized to the value for 55° and the theoretical estimate of the optimal scale length for RA, respectively. The result shows that the normalized plasma scale length for the best $K\alpha$ yield of these two materials is almost the same.

In addition, Fig. 10 essentially shows the relationship between scale length and α_{\max} , the angle at which RA is optimized. The optimal prepulse delay increases with decreasing

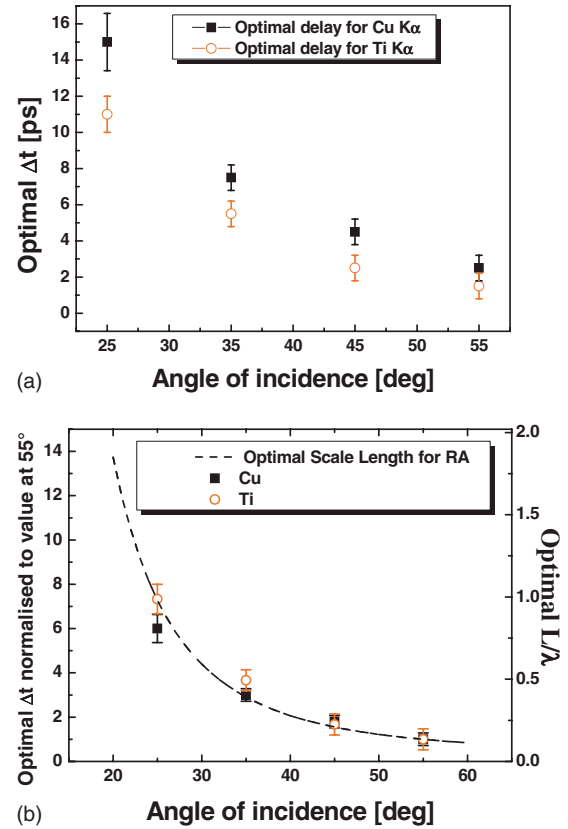


FIG. 10. (Color online) (a) Shows the optimal delay time for the prepulse to have the maximum $K\alpha$ emission, extracted from Fig. 6. (b) Normalization the experimental data and theoretical calculation of the optimal plasma scale length for resonance absorption (dashed curve, Y axis on the right-hand side). The theoretical curve is estimated from $(2\pi L/\lambda)^{2/3} \sin^2 \theta = 0.6$ (Ref. [33]).

angle of incidence since the optimum plasma scale length for maximum RA increases with decreasing angle of incidence. For a long scale length (e.g., $L/\lambda \approx 1$), a small α_{\max} ($\approx 25^\circ$) should lead to efficient $K\alpha$ generation; short scale lengths (e.g., $L/\lambda \approx 0.1$) lead to a correspondingly large α_{\max} ($\approx 55^\circ$). Thus, if in an experiment, the scale length is given, then one should adjust the angle of incidence to α_{\max} to obtain the maximum $K\alpha$ yield. Or vice versa: if α is fixed, then one has to lengthen or shorten L accordingly via prepulse control. Such an optimization could be achieved at least in the range of the values of α and L (obtained from Δt) covered by the current experiment, i.e., $\alpha \sim 25^\circ \dots 55^\circ$ and $L/\lambda \sim 0.1 \dots 1$.

Thus, according to both horizontal lines in Fig. 9, we may conclude that for a given contrast ratio (given by the laser system) and ion mass or a given scale length in the experiment, $K\alpha$ generation can be optimized when the angle of incidence α is chosen appropriately.

But we also would like to make a practical note. Although optimized conditions at large angle of incidence (e.g., $\alpha = 80^\circ$) lead to the same amount of $K\alpha$ photons as for a small angle (e.g., $\alpha = 20^\circ$, also with optimized prepulse conditions), due to the required constant intensity on target surface, one needs to have a significant larger energy within the laser pulse [in this example a factor $\cos(20^\circ)/\cos(80^\circ) \sim 5$ times more for $\alpha = 80^\circ$].

Another issue for applications is that at a large incidence angle the $K\alpha$ source size will be significantly larger, and hence reduce the resolving power for experiments such as TRXD. For these reasons, using a controlled prepulse to generate an artificial plasma scale length for optimization the absorption conditions at small angles of incidence may be the better option.

V. PIC SIMULATIONS

To obtain a more quantitative picture of the $K\alpha$ production, it is first necessary to determine the energies and numbers of hot electrons generated by laser heating, and then calculate the $K\alpha$ -photon yield produced by fast electrons going inside the targets. The discussion above assumes that resonance absorption is the dominant mechanism of hot-electron production, which is only valid as long as the density scale length exceeds the excursion length of electrons oscillating in the laser field: $L > v_{\text{osc}}/\omega$, where $v_{\text{osc}}/c \approx 0.83 (I\lambda^2/10^{18} \text{ W cm}^{-2} \mu\text{m}^2)^{1/2}$ and ω is the laser frequency. The laser intensities and high-contrast ratios used in this experiment suggest that this inequality will be violated for the smaller prepulse delays, so to avoid this restriction we performed detailed particle-in-cell simulations using the 1D3V code BOPS [16,36]. The simulations used up to 6000 cells and 500 000 electrons and ions, employing the relativistic boost technique to treat obliquely incident, p -polarized light.

The initial plasma parameters were chosen as close as possible to those expected in the experiment. A rough estimate of the preplasma electron temperature based on the results of Ref. [37] gives a value $T_e = 0.5$ keV. The maximum prepulse delay chosen in the experiment was 25 ps, assuming that $L \equiv Cs\Delta t$ gives a maximum scale-length $L/\lambda = 1.0$ for titanium. In the simulations scale lengths were chosen from $L/\lambda = 0.01$ to $L/\lambda = 0.9$. The effective normalized mass-to-charge ratios (M/Zm_e) for titanium and copper were 8730 and 11570, respectively, corresponding to an effective ionization degree $Z = 10$ for both elements. This choice allowed the same range of scale lengths for both targets. The initial density profiles were set up to keep the *total mass of the target constant*; thus, whereas the foils with $L/\lambda = 0.01$ had a maximum density $n_e/n_c = 32$ and thickness $0.35 \mu\text{m}$ for titanium, and $n_e/n_c = 48.7$ and thickness $0.36 \mu\text{m}$ for copper. The long scale-length case had $n_e/n_c = 13.3$, thickness $5.1 \mu\text{m}$ and $n_e/n_c = 20.3$, thickness $5.48 \mu\text{m}$ for titanium and copper, respectively. The energy distributions of hot electrons absorbed by the right-hand side boundary of the simulation box (rear side of the target) were collected to determine their characteristic energy and the overall energy absorbed. The dependence of absorbed energy on the plasma scale length is shown in Fig. 11.

As expected from the simple resonance absorption (RA) analysis earlier (Fig. 10), one can immediately see a broad qualitative correlation with the experimental $K\alpha$ yields in Fig. 6. For smaller incidence angles, the peak absorption fraction shifts to longer density scale lengths (which we assume to scale linearly with the prepulse delay). Note, however, that contrary to RA theory, the absorption (which is purely collisionless here) does not drop to zero for pure step

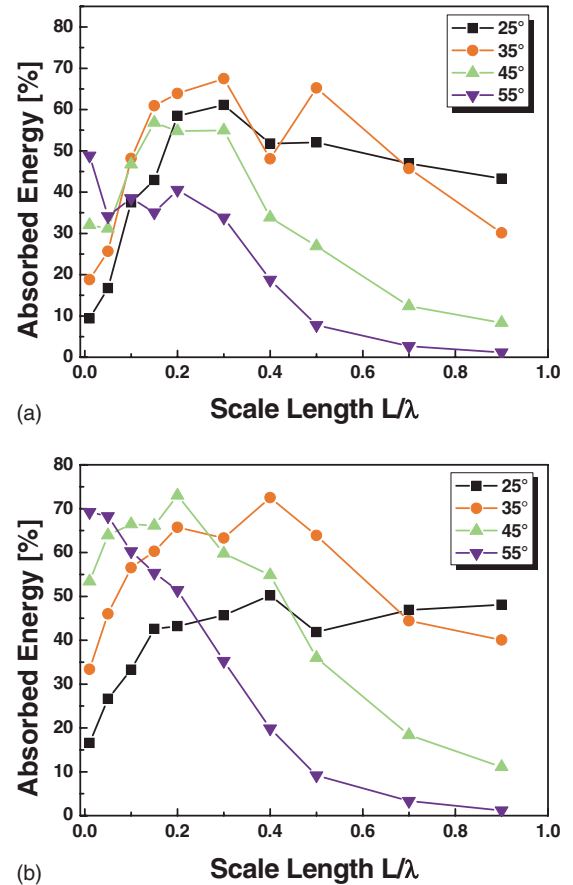


FIG. 11. (Color online) Calculated laser energy absorbed by hot electrons as a function of the initial plasma density scale length and incidence angle for (a) Cu and (b) for Ti targets.

profiles, but follows the typical pattern for vacuum heating [15,16], exhibiting a maximum at large incidence angles ($45\text{--}70^\circ$).

The total number of $K\alpha$ photons generated by the hot electrons during their propagation through the solid-state matter of the target was calculated according to a standard cross-section model in a manner similar to Refs. [10,38]. For this purpose, the electron distributions obtained from the PIC simulations are split into 200 monoenergetic beams, which are then treated separately. The foil is divided into 200 cells and for each energy group the electrons are transported through the cell, using the relativistic K -shell ionization cross section [39] to calculate the number of $K\alpha$ photons generated. Each electron beam is slowed down via collisions according to the Bethe stopping formula, whereby the stopping power is taken from the NIST database [40] for both materials. Once the electron beam escapes from the rear of the target it is assumed to play no further role in the $K\alpha$ photons production, a reasonable simplification since the foils were mounted on low Z (glass) substrates. The reabsorption of $K\alpha$ photons is also accounted for according to the thickness of the cell in the foil. The attenuation coefficient is taken also from the NIST database [41].

Figure 12 shows the $K\alpha$ -yield dependence on the initial density scale length. It is clear from Figs. 12(a) and 12(b) that the qualitative behavior is the same for the both materi-

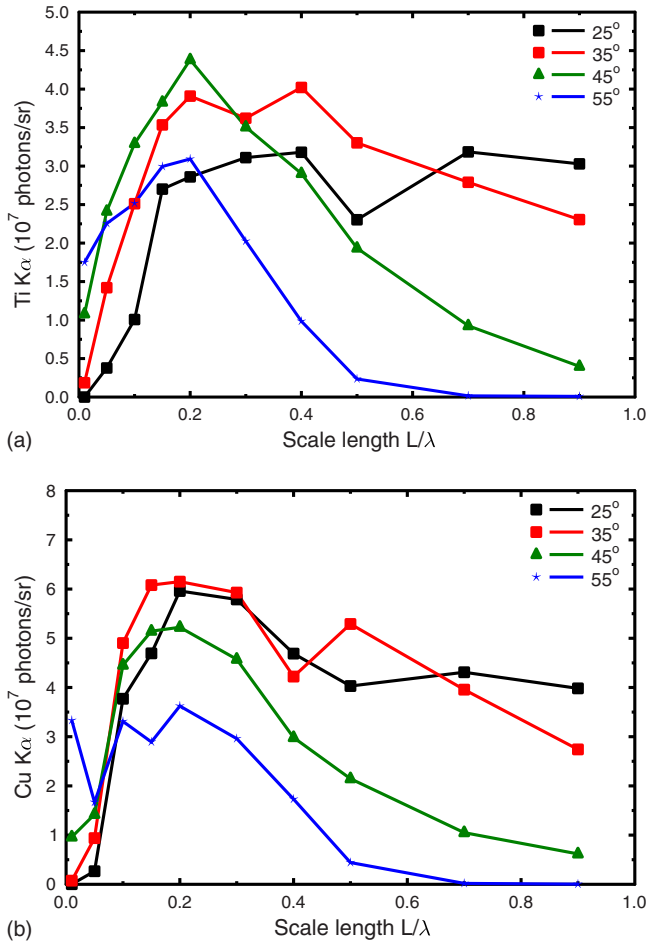


FIG. 12. (Color online) Simulated $K\alpha$ yield per pulse as a function of the initial plasma density scale length and incidence angle for (a) Ti and (b) Cu targets.

als as in the experiment. The $K\alpha$ yield reaches its maximum for roughly the same scale length as the absorption of incoming laser energy, indicating that the value of $K\alpha$ yield is largely determined by the absorption efficiency in this case. On the other hand, the absolute values of $K\alpha$ yields obtained from the PIC simulations are a factor of three to four times lower than the measured values, a discrepancy which could be due in part to the geometrical simplifications in the model. There are also differences in the positions and values of the $K\alpha$ maxima, although these are difficult to define precisely for the simulations because of insufficient statistics.

Although the absolute $K\alpha$ maxima vary by more in the simulations than in the experiment (50% fluctuation vs $\sim 10\%$), it is still interesting to compare these values (across all scale lengths) with the value obtained for $L/\lambda=0.01$ (i.e., effectively no prepulse). The results of this analysis displayed in Fig. 13 confirm the interpretation offered earlier for the trend seen in Fig. 9: namely, that the main pulse itself causes significant and rapid expansion of the density profile. The discrepancy in the crossover angle (here 90° for Ti vs the observed 62°) is likely due to a higher mass: charge ratio for the ions in the PIC simulations than is actually present in the experiments. This angular-dependent shelf expansion effect is consistent with earlier PIC studies of profile modifi-

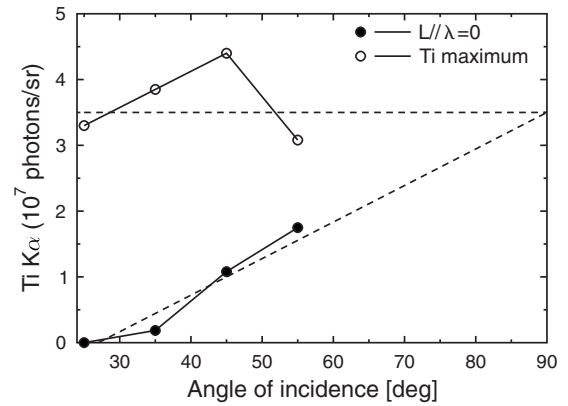


FIG. 13. Comparison of simulated maximum Ti $K\alpha$ yield per pulse and yield for a density scale-length $L/\lambda=0.01$ (no prepulse).

cation at oblique incidence angles, in which ions tend to be dragged out back toward the laser by hot electrons circulating at the front of the target [42,43]. Figure 9 thus represents a clear experimental confirmation of this phenomenon, independent of direct ion energy spectra measurements.

VI. CONCLUSIONS

In summary, it has been demonstrated that for a range of conditions typical for laser systems with moderate to high-contrast ratios, i.e., for a steep density gradient ($L/\lambda \sim 0.1$) or even in the presence of an extended density shelf ($L/\lambda \sim 1$), the $K\alpha$ emission of a femtosecond-laser plasma could be optimized.

In particular, using carefully prepared solid-density targets and clean interaction conditions with intense ($I_L \sim 10^{16} \text{ W/cm}^2 - 10^{17} \text{ W/cm}^2$) 150-fs laser pulses, the yield of $K\alpha$ photons of Cu and Ti targets was measured at different angles of incidence and different prepulse conditions. It has been shown that for constant laser intensity on a steep density gradient plasma, $K\alpha$ -emission yield is highest at large angle of incidence, (here $\alpha \sim 80^\circ$). For smaller angles the yield steadily decreases and reaches its lowest value when approaching normal incidence. However, introducing a prepulse at appropriate time in advance to the main pulse, the yield can be optimized to the same value as at large angle of incidence without prepulse and hence the $K\alpha$ yield can be optimized to the same value *independently* of the angle of incidence. Experimentally this was verified for $\alpha \sim 25^\circ$ to 55° .

Physically this situation can be described by optimization of the absorption, which for the present experimental conditions is mostly resonant absorption or some similar collisionless process. Because $K\alpha$ generation is more or less directly proportional to the absorption—as supported by the present simulations—optimization of the absorption is equivalent to optimization of the production of $K\alpha$ photons. As has been shown, both, using classical RA model from Ginzburg or PIC simulations, the angle of incidence where this absorption peaks is strongly dependent on the scale length. For heavier ions, such as Cu, the scale length is directly proportional to the delay between prepulse and main pulse. Thus for each

angle of incidence there is an optimum for prepulse delay: large delay (or scale length) for a small angle or short delay or even no prepulse (steep gradient plasma) when the angle of incidence is large.

For ions with somewhat lower mass, in principle the situation is similar. However, due to the lower mass, even a small prepulse or the leading edge even of a high-contrast main pulse, could lead to a small density shelf. Thus a small scale length is present, even in the absence of an additional prepulse. Then the optimum condition for $K\alpha$ generation is a somewhat smaller angle, e.g., 60° for Ti in the present experiment. This experimental observation is supported by PIC simulations on laser-pulse absorption, hot-electron generation and postprocessing of electron transport and $K\alpha$ production.

For practical and economic purposes, these findings suggest using a small angle of incidence and matched Δt : first, this requires less energy to achieve the same on-target intensity and second, gives a smaller source size which is advantageous for many experiments. Smaller incidence angles may be even more advantageous, but this could not be confirmed

here because the experimental setup was restricted to $\alpha > 25^\circ$.

On the other hand, the present work indicates that for density scale lengths created by typical prepulse given by the contrast of the laser system and other experimental conditions (within the range $L/\lambda \sim 0.1-1.0$), the $K\alpha$ yield could be optimized by operating the x-ray source at the matched angle of incidence. Experimental arrangements in which an unintentional (or unavoidable) prepulse is present could probably be improved simply by using a small angle of incidence instead of the 45° geometry typical of many setups: the present study indicates that the x-ray photon count could be increased by a factor of 2 or 3 in this case, with obvious advantages for many applications of fs- $K\alpha$ sources, such as TRXD.

ACKNOWLEDGMENTS

This work was supported by the Deutsche Forschungsgemeinschaft (Contract No. SFB 616 and Grants No. GI 300/3-1, No. TE 190/6-1, and No. So 408/6-3) and the European Union (Marie-Curie-network *FLASH*).

-
- [1] T. Feurer, A. Morak, I. Uschmann, Ch. Ziener, H. Schwörer, E. Förster, and R. Sauerbrey, *Appl. Phys. B: Lasers Opt.* **72**, 15 (2001).
- [2] Z. Jiang, J. C. Kieffer, J. P. Matte, M. Chaker, O. Peyrusse, D. Gilles, G. Korn, A. Maksimchuk, S. Coe, and G. Mourou, *Phys. Plasmas* **2**, 1702 (1995).
- [3] D. D. Meyerhofer, H. Chen, J. A. Delettrez, B. Soom, S. Uchida, and B. Yaakobo, *Phys. Fluids B* **5**, 2584 (1993).
- [4] P. Gibbon and E. Förster, *Plasma Phys. Controlled Fusion* **38**, 769 (1996).
- [5] Ch. Reich, P. Gibbon, I. Uschmann, and E. Förster, *Phys. Rev. Lett.* **84**, 4846 (2000).
- [6] F. Ewald, H. Schwoerer, and R. Sauerbrey, *EPL* **60**, 710 (2002).
- [7] D. C. Eder, G. Pretzler, E. Fill, K. Eidmann, and A. Saemann, *Appl. Phys. B: Lasers Opt.* **70**, 211 (2000).
- [8] U. Teubner, C. Wülker, W. Theobald, and E. Förster, *Phys. Plasmas* **2**, 972 (1995).
- [9] for example, C. Rischel, A. Rouse, I. Uschmann, P.-A. Albouy, J.-P. Geindre, P. Audebert, J.-C. Gauthier, E. Fröster, J.-L. Martin, and A. Antonetti, *Nature (London)* **390**, 490 (1997); C. Rose-Petruck, R. Jimenez, T. Guo, A. Cavalleri, C. W. Siders, F. Raksi, J. A. Squier, B. C. Walker, K. R. Wilson, and C. P. J. Barty, *ibid.* **398**, 310 (1999); K. Sokolowski-Tinten, C. Blome, J. Blums, A. Cavalleri, C. Dietrich, A. Tarasevitch, I. Uschmann, E. Förster, M. Kammler, M. Horn-von Hoegen, and D. von der Linde, *ibid.* **422**, 287 (2003); M. Bargheer, N. Zhavoronkov, Y. Gritsai, J. C. Woo, D. S. Kim, M. Woerner, and T. Elsaesser, *Science* **306**, 1771 (2004).
- [10] D. Salzmann, Ch. Reich, I. Uschmann, and E. Förster, *Phys. Rev. E* **65**, 036402 (2002).
- [11] A. Zhidkov, A. Sasaki, T. Utsumi, I. Fukumoto, T. Tajima, F. Saito, Y. Hironaka, K. G. Nakamura, K. I. Kondo, and M. Yoshida, *Phys. Rev. E* **62**, 7232 (2000).
- [12] F. Y. Khattak, E. Garcia Saiz, T. Dzelzainis, D. Riley, and Z. Zhai, *Appl. Phys. Lett.* **90**, 081502 (2007).
- [13] Ch. Reich, I. Uschmann, F. Ewald, S. Düsterer, A. Lübcke, H. Schwoerer, R. Sauerbrey, E. Förster, and P. Gibbon, *Phys. Rev. E* **68**, 056408 (2003).
- [14] Ch. Ziener, I. Uschmann, G. Stobrawa, Ch. Reich, P. Gibbon, T. Feurer, A. Morak, S. Düsterer, H. Schwoerer, E. Förster, and R. Sauerbrey, *Phys. Rev. E* **65**, 066411 (2002).
- [15] F. Brunel, *Phys. Rev. Lett.* **59**, 52 (1987).
- [16] P. Gibbon and A. R. Bell, *Phys. Rev. Lett.* **68**, 1535 (1992).
- [17] U. Teubner, J. Bergmann, B. van Wonterghem, F. P. Schäfer, and R. Sauerbrey, *Phys. Rev. Lett.* **70**, 794 (1993).
- [18] U. Teubner, P. Gibbon, E. Förster, F. Falliès, P. Audebert, J. P. Geindre, and J. C. Gauthier, *Phys. Plasmas* **3**, 2679 (1996).
- [19] U. Teubner, W. Theobald, and C. Wülker, *J. Phys. B* **29**, 4333 (1996).
- [20] F. Y. Khattak, O. A. M. B. Percie du Sert, D. Riley, P. S. Foster, E. J. Dival, C. J. Hooker, A. J. Langley, J. Smith, and P. Gibbon, *Phys. Rev. E* **74**, 027401 (2006).
- [21] N. Zhavoronkov, Y. Gritsai, M. Bargheer, M. Woerner, and T. Elsaesser, *Appl. Phys. Lett.* **86**, 244107 (2005).
- [22] H. Nakano, T. Nishikawa, and N. Uesugi, *Appl. Phys. Lett.* **79**, 24 (2001).
- [23] H. Ahn, H. Nakano, T. Nishikawa, and N. Uesugi, *Jpn. J. Appl. Phys., Part 2* **35**, L154 (1996).
- [24] T. Feurer, *Appl. Phys. B: Lasers Opt.* **68**, 55 (1999).
- [25] U. Teubner, G. Kühnle, and F. P. Schäfer, *Appl. Phys. B: Photophys. Laser Chem.* **54**, 493 (1992).
- [26] S. Bastiani, A. Rouse, J. P. Geindre, P. Audebert, C. Quoix, G. Hamoniaux, A. Antonetti, and J.-C. Gauthier, *Phys. Rev. E* **56**, 7179 (1997).
- [27] Th. Schlegel, S. Bastiani, L. Grèmmillet, J.-P. Geindre, P. Aude-

- bert, J.-C. Gauthier, E. Lebeuvre, G. Bonnaud, and J. Delettrez, *Phys. Rev. E* **60**, 2209 (1999).
- [28] F. Zamponi, T. Kämpfer, A. Morak, I. Uschmann, and E. Förster, *Rev. Sci. Instrum.* **76**, 116101 (2005).
- [29] The quantum efficiency of the CCD was calibrated with a Si reference detector.
- [30] K. Sokolowski-Tinten, C. Blome, J. Blums, A. Cavalleri, C. Dietrich, A. Tarasevitch, and D. von der Linde, *AIP Conf. Proc.* **634**, 11 (2002).
- [31] H.-S. Park, D. M. Chambers, H.-K. Chung, R. J. Clarke *et al.*, *Phys. Plasmas* **13**, 056309 (2006).
- [32] R. Rix, *Diplomarbeit* (Max-Planck-Institut Für Quantenoptik, Garching, Germany, 1999).
- [33] W. L. Kruer, *The Physics of Laser Plasma Interaction* (Addison-Wesley, Redwood City, CA, 1988).
- [34] U. Teubner, I. Uschmann, P. Gibbon, D. Altenbernd, E. Förster, T. Feurer, W. Theobald, R. Sauerbrey, G. Hirst, M. H. Key, J. Lister, and D. Neely, *Phys. Rev. E* **54**, 4167 (1996).
- [35] A. Tarasevitch, A. Orisch, D. von der Linde, Ph. Balcou, G. Rey, J.-P. Chambaret, U. Teubner, D. Klöpfel, and W. Theobald, *Phys. Rev. A* **62**, 023816 (2000).
- [36] P. Gibbon, A. Andreev, E. Lefebvre, and G. Bonnaud, *Phys. Plasmas* **6**, 947 (1999).
- [37] G. Guethlein, M. E. Foord, and D. Price, *Phys. Rev. Lett.* **77**, 1055 (1996).
- [38] D. Riley, J. J. Angulo-Gareta, F. Y. Khattak, M. J. Lamb, P. S. Foster, E. J. Divall, C. J. Hooker, A. J. Langley, R. J. Clarke, and D. Neely, *Phys. Rev. E* **71**, 016406 (2005).
- [39] C. A. Quarles, *Phys. Rev. A* **13**, 1278 (1976).
- [40] International Commission on Radiation Units & Measurements Report No. 37, 1984 (unpublished).
- [41] <http://physics.nist.gov/PhysRefData/XrayMassCoef/cover.html>
- [42] P. Gibbon, *Phys. Rev. Lett.* **73**, 664 (1994).
- [43] R. J. Kingham, P. Gibbon, W. Theobald, L. Veisz, and R. Sauerbrey, *Phys. Rev. Lett.* **86**, 810 (2001).